PCCP

PAPER

View Article Online
View Journal | View Issue

Cite this: *Phys. Chem. Chem. Phys.*, 2014, **16**, 12688

Characterization of organic fluorophores for *in vivo* FRET studies based on electroporated molecules†

A. Plochowietz,* R. Crawford‡ and A. N. Kapanidis

Received 7th March 2014,
Accepted 28th April 2014

DOI: 10.1039/c4cp00995a

www.rsc.org/pccp

In vivo single-molecule fluorescence and Förster resonance energy transfer (FRET) techniques are excellent tools for studying spatial distribution, the nanoscale structure and conformational changes in living cells. We have recently introduced an electroporation-based method to internalize DNA and proteins labeled with organic fluorophores into living bacteria and established the ability for long-lived single-molecule fluorescence and FRET measurements. However, further developments, such as optimization of electroporation conditions, evaluation of organic fluorophore performance *in vivo* and quantitative single-cell FRET analysis, are needed to make the method more robust and general. Using singly-labeled DNA fragments, we optimized internalization efficiency and cell viability at six electroporation voltages, achieving >60% loading and viability similar to non-treated cells. We characterized the photostability and brightness of three donor fluorophores and four acceptor fluorophores *in vivo*; Cy3B, Atto647 and Atto647N performed best with photobleaching lifetimes of ~20 s, 46 s and 92 s, respectively, and brightness values of ~4000 photons per second under the same illumination conditions. We used three doubly-labeled DNA FRET standards (having *in vitro* FRET efficiencies of ~17%, ~42%, and ~88%) and an alternating-laser excitation scheme to measure apparent FRET efficiencies at the single-cell level. We showed that we could differentiate DNA FRET standards at the single-cell level. Our approach offers a powerful method for the study of intramolecular changes or complex formation using FRET at the single-cell level in live bacteria.

Introduction

Single-molecule fluorescence studies have been used to investigate the protein copy number, localization and diffusion patterns within the cell and have helped to understand cellular processes such as gene expression, regulation and membrane transport.[2] Single-molecule Förster resonance energy transfer (FRET) studies can measure conformational changes at the biologically relevant length scale of 2–10 nm with a resolution of ~0.5 nm and have been used for instance to elucidate protein folding[3] and conformational states of enzymes.[4,5]

However, single-molecule fluorescence and especially FRET studies are often limited to *in vitro* conditions, since the labeled protein of interest has to be introduced into the living cell or has to be labeled inside the living cell. The latter is employed in most single-molecule fluorescence studies by fusing the protein of interest with fluorescent proteins (FPs) such as the green fluorescent protein and its variants.[6,7] But FPs are limited by their lower brightness and photostability compared to their organic fluorophore counterparts.[6,8] First, the higher photon budget and slower photobleaching rates make organic fluorophores better suited for single-molecule tracking studies than FPs. Second, organic fluorophores are the better option for FRET studies, since they are 100-fold smaller in volume and offer easier intra-molecular labeling *via* cysteine mutations than FPs. *In vivo* single-molecule FRET studies become possible by tagging the protein of interest with the favorable organic fluorophores *in vitro* and then delivering the specifically labeled protein into the living cell.

Internalization methods such as scrape loading,[9] syringe loading,[10] and microinjection[11] have been presented for eukaryotic cells. In 2010, single-molecule FRET measurements using microinjection of proteins labeled with organic fluorophores into live mammalian cells were reported.[12] This method is not applicable to bacterial cells due to their small size (*E. coli*: 1–3 μm, microinjection needle diameter: 1 μm) and persistent cell walls. Internalization methods such as endocytosis, heat shock,[13] electroporation,[14] sonoporation[15] and detergent treatment[16] have been used to internalize short DNA fragments into bacterial cells.

Clarendon Laboratory, Department of Physics, Parks Road, Oxford, OX1 3PU, UK. E-mail: anne.plochowietz@physics.ox.ac.uk

† Electronic supplementary information (ESI) available: Supplementary information on materials and methods as well as 7 supplementary figures. See DOI: 10.1039/c4cp00995a

‡ Current address: Illumina, Chesterford Research Park, Little Chesterford, CB10 1XL, UK

We recently, presented a versatile and high-throughput method to internalize 45-bp DNA fragments and proteins of up to 100 kDa labeled with organic fluorophores into *E. coli* by employing electroporation.[1] In this proof-of-principle study, we were able to count the number of internalized molecules per cell and achieved loading of up to 1000 molecules per cell. Aided by the brightness and photostability of the organic fluorophores, we were able to extend single-molecule tracking to 10 s and obtained a fluorescence observation time of 10 min in live cells – extending observation time in fluorescence studies by at least 10-fold compared to FP-based studies. Moreover, we performed initial single-molecule FRET studies of localized molecules in live *E. coli*.

However, further characterization, such as a trade-off between cell viability and cell loading at different electroporation voltages as well as the characterization of suitable organic fluorophores for *in vivo* FRET studies are needed to make the method more robust and applicable.

Here, we used singly-labeled 45-bp dsDNA standards to study cell viability and internalization efficiency at six electroporation voltages; we also showed that we can achieve a good compromise between cell viability comparable to non-treated cells and cell loading. In order to study organic fluorophore properties *in vivo*, we internalized DNA standards singly-labeled with three donor fluorophores and four acceptor fluorophores into *E. coli*. We performed single-cell photobleaching measurements of heavily loaded cells to obtain fluorophore photostability and performed single-cell photobleaching analysis with single-molecule sensitivity to obtain the fluorophore brightness. We evaluated the performance of the organic fluorophores and selected promising FRET dye pairs for further studies. Using an alternating laser excitation scheme, we also measured apparent FRET efficiencies at the single-cell level for low, intermediate and high DNA FRET standards (Fig. S1, ESI†) and we were able to distinguish DNA FRET standards at the single-cell level; providing an easy assay to study intramolecular changes or complex formation using FRET at an ensemble level. This study should serve as a reference for choosing the electroporation voltage, organic fluorophores and FRET dye pairs depending on the application of interest and aid in applying the electroporation-based internalization method to study biological processes in bacteria using *in vivo* single-molecule fluorescence and FRET measurements.

Results

For internalization of DNA molecules into live bacteria *via* electroporation (Fig. 1A), we added the labeled DNA standards to electrocompetent cells and exposed the cell suspension to the discharge of a high-voltage electric field. Transient pores were formed through which the labeled DNA molecules could

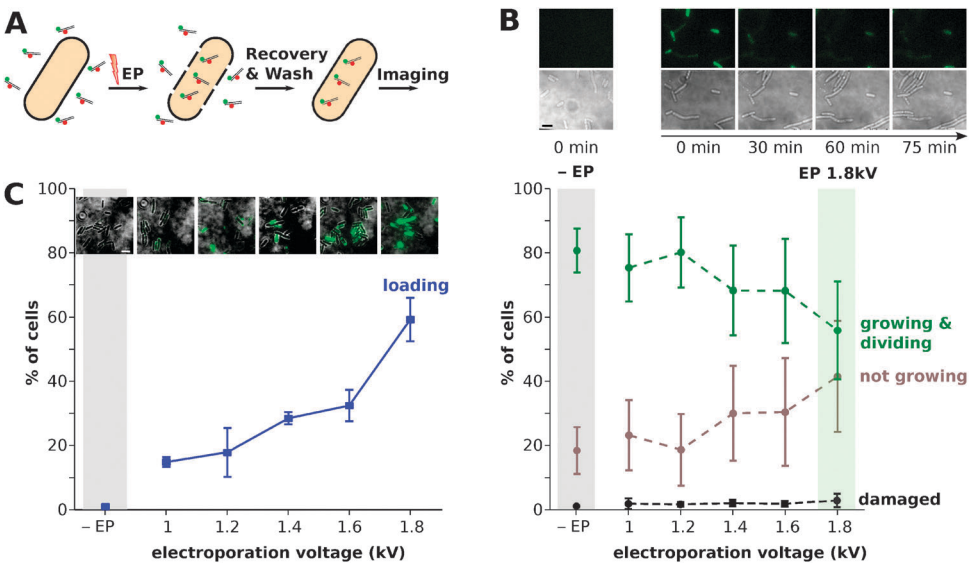

Fig. 1 Cell viability and cell loading dependent on electroporation. (A) An electroporation schematic. Electrocompetent cells and doubly-labeled dsDNA are exposed to the discharge of a high-voltage electric field (electroporation, EP). Labeled dsDNA enters the cells through transient pores. Cells are recovered and non-internalized dsDNA is washed off before imaging. (B) Characterization of cell viability dependent on the applied electroporation voltage. Top: images of non-electroporated cells (left, negative control) and electroporated cells at 1.8 kV over 75 min at 37 °C (right); fluorescence and brightfield images are shown. Growth and division of cells is monitored as a measure of viability. Bottom: percentage of cells showing growth and division, retaining their shape (not growing) and showing compromised membranes (damaged) at 6 different electroporation voltages (-EP, 1 to 1.8 kV). The percentage of growing and dividing cells drops from (81 ± 7)% without EP under the imaging conditions down to (56 ± 15)% under the harshest condition of 1.8 kV, but the percentage of damaged cells stays below 3%. (C) Characterization of cell loading dependent on the applied electroporation voltage. Inset images: an overlay of inverted brightfield and fluorescence images of example FOVs of cells electroporated at 0 to 1.8 kV (left to right). A clear increase in loading (blue curve) from (15 ± 2)% at 1.0 kV to (60 ± 7)% at 1.8 kV was observed; cells were considered as loaded when the initial cell intensity normalized by the cell area was larger than the mean plus three times the standard deviation (stdev) of non-electroporated cells. The graphs in B and C show the mean and stdev of 3 data sets; 1 data set: 300–500 cells per electroporation voltage. Scale bar: 3 μm.

enter the cell. The cells were quickly recovered in a rich medium and the non-internalized DNA molecules were washed off before imaging (ESI†).

Dependence of cell viability and loading on electroporation voltage

First, we electroporated 2 μM singly-labeled dsDNA-Cy3B into *E. coli* and checked the dependence of cell viability on the applied electroporation voltage. For measuring cell viability, we followed the growth and division of cells in the brightfield image over the course of up to 1.5 h and classified cells as 'growing & dividing', 'not growing' and 'damaged'. Cells were classified as 'damaged' if they showed a compromised cell membrane in the brightfield image and cells were classified as 'not growing' if they looked intact but did not grow or divide during our observation time.

Under our imaging conditions, rich medium agarose pads heated to 37 °C, we observed (81 ± 7)% of 'growing & dividing' cells in our non-electroporated sample (Fig. 1B, gray bar). With increasing electroporation voltage, we observed a decrease in percentage of 'growing & dividing' cells and an increase in percentage of 'not growing' cells (Fig. 1B, bottom). However, we observed less than 3% of 'damaged' cells at all electroporation voltages. Under the harshest electroporation conditions of 1.8 kV, we still observed (56 ± 15)% of 'growing and dividing' cells and obtained a viability of ~70% at 1.4 kV and 1.6 kV. The 3 data sets at each electroporation voltage were obtained on three different days and the large error bars of up to 15% show large sample-to-sample variations. Furthermore, the time window of observation after recovery is important, since cells might show different lag-times after electroporation where the cells will not divide and thus would be classified as 'not growing' using this viability assay.

Second, we studied cell loading due to internalization of 2 μM singly-labeled dsDNA-Cy3B at six different electroporation voltages. In the green fluorescence channel we could already see a clear increase of loaded cells with an increase in electroporation voltage (Fig. 1C, inset images). Under these imaging conditions, (14.8 ± 1.5)% of cells were loaded at 1.0 kV and about 30% of the cells were loaded at 1.4 kV and 1.6 kV (Fig. 1C). Here, we used a conservative loading threshold where cells were classified as loaded when the overall cell intensity normalized by the cell area was larger than the mean plus three times the standard deviation of non-electroporated cells. Using this loading threshold only (0.6 ± 0.4)% of non-electroporated cells were classified as loaded, despite the higher autofluorescence of the cells in the green fluorescence channel (Fig. 1C, gray bar). For further studies, we used an electroporation voltage of 1.4 kV, which offers a good compromise between sufficient cellular loading and high cell viability.

Photostability of organic fluorophores *in vivo*

Next, we evaluated the photostability and brightness of 7 organic fluorophores for their use in *in vivo* FRET studies. For simplicity, we present the photostability and brightness analysis for two

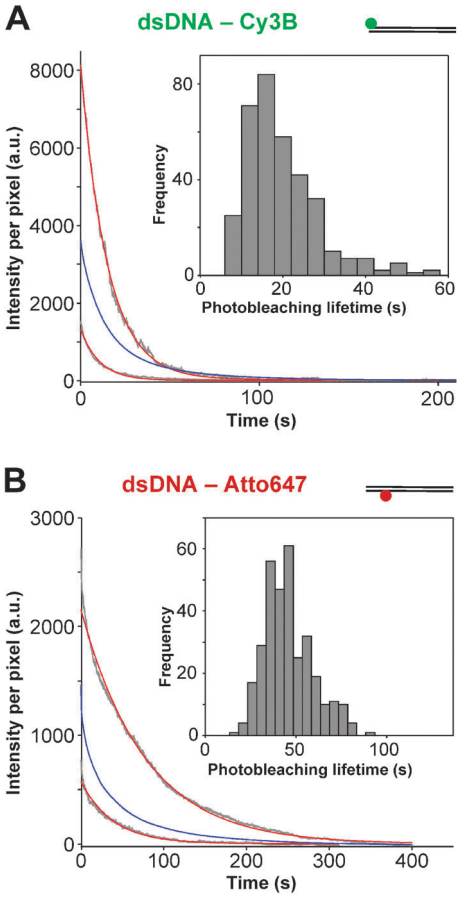

Fig. 2 Photostability study of organic fluorophores *in vivo*. (A) Single-cell photobleaching study of internalized dsDNA-Cy3B into live *E. coli* as a measure for photostability. Main: two examples of single-cell photobleaching timetraces (gray), the single-exponential fit of timetraces (red) and the average single-cell photobleaching timetrace (blue). Inset: a histogram of photobleaching lifetime obtained by the single-exponential fit of single-cell photobleaching timetraces. (B) Single-cell photobleaching lifetime measurements of dsDNA-Atto647 (Main and inset as described in A). Acceptor fluorophore Atto647 showed a photobleaching lifetime of (46 ± 13; 44) s, whereas donor fluorophore Cy3B showed a photobleaching lifetime of (20 ± 9; 17) s; (mean ± stdev; median). Each data set consists of 300–600 cells.

example organic fluorophores Cy3B (green fluorescence channel) and Atto647 (red fluorescence channel). A similar analysis for Cy3 and Atto532 (green fluorescence channel), and Cy5, Alexa647, and Atto647N (red fluorescence channel) can be found in the ESI† (Fig. S2, S3, S5 and S6, respectively).

We used the single-cell photobleaching lifetime of heavily loaded cells as a measure for photostability of the organic fluorophore *in vivo*. Therefore, we electroporated cells with a 1 μM concentration of singly-labeled dsDNA-Cy3B and dsDNA-Atto647, respectively, and carried out single-cell photobleaching studies. The fluorescence decay of the total cell intensity normalized by the cell area was measured and single-cell photobleaching timetraces were obtained (Fig. 2, gray curves: raw data). The raw single-cell photobleaching timetraces were fitted with a single-exponential (Fig. 2, red curves: fit), since the photobleaching lifetime of the agarose pad/background itself was less than 1 s

and thus neglectable (Fig. S2A and S3A, ESI†). We obtained a photobleaching lifetime for Cy3B of (20 ± 9) s, median: 17 s, and for Atto647 of (46 ± 13) s, median: 44 s. An extremely large photobleaching lifetime of (92 ± 37) s, median: 86 s, was obtained for Atto647N (Fig. S3D, ESI†).

We also electroporated the fluorescent protein mCherry into live *E. coli* and after the same analysis obtained a photobleaching lifetime of (18 ± 5) s, median: 17 s, showing that the photostability of organic fluorophores and fluorescent proteins is similar under these illumination conditions (Fig. S4, ESI†).

Brightness of organic fluorophores *in vivo*

We used the characteristic steps in single-cell photobleaching timetraces of sparsely loaded cells as a measure of fluorophore brightness *in vivo*. Therefore, we electroporated *E. coli* with a 10–30 nM concentration (30–100 times lower than in photostability studies) of singly-labeled dsDNA-Cy3B and dsDNA-Atto647 to be able to observe single molecules inside the cells. Cells loaded with less than 6 fluorescent molecules were used for further analysis; single-step photobleaching timetraces were fitted by Hidden Markow Modeling (HMM) as previously described[1] and the photobleaching step heights were obtained

Table 1 Comparison of organic fluorophore photostability and brightness of 3 donor (green channel) and 4 acceptor (red channel) fluorophores. Photostability analysis is shown in Fig. 2 and Fig. S2 and S3, ESI and brightness analysis is shown in Fig. 3 and Fig. S5 and S6, ESI. A visualization of the results is shown in Fig. S7, ESI. The evaluation of the fluorophore performance in *in vivo* single-molecule fluorescence/FRET studies is based on both high photostability and high brightness; '++': very good, '+': good, '−': poor

	Photostability	Brightness	
Organic fluorophore	Photobleaching lifetime (s)	Single-molecule unitary intensity (ph s^{-1})	Performance
Green channel			
Cy3B	20 ± 9	3400 ± 1500	++
Cy3	18 ± 7	2800 ± 1100	+
Atto532	14 ± 8	3600 ± 1400	+
Red channel			
Atto647	46 ± 13	3400 ± 1100	++
Cy5	10 ± 5	4500 ± 1500	+
Alexa647	6 ± 4	3500 ± 1200	−
Atto647N	92 ± 37	3500 ± 1300	++, sticky

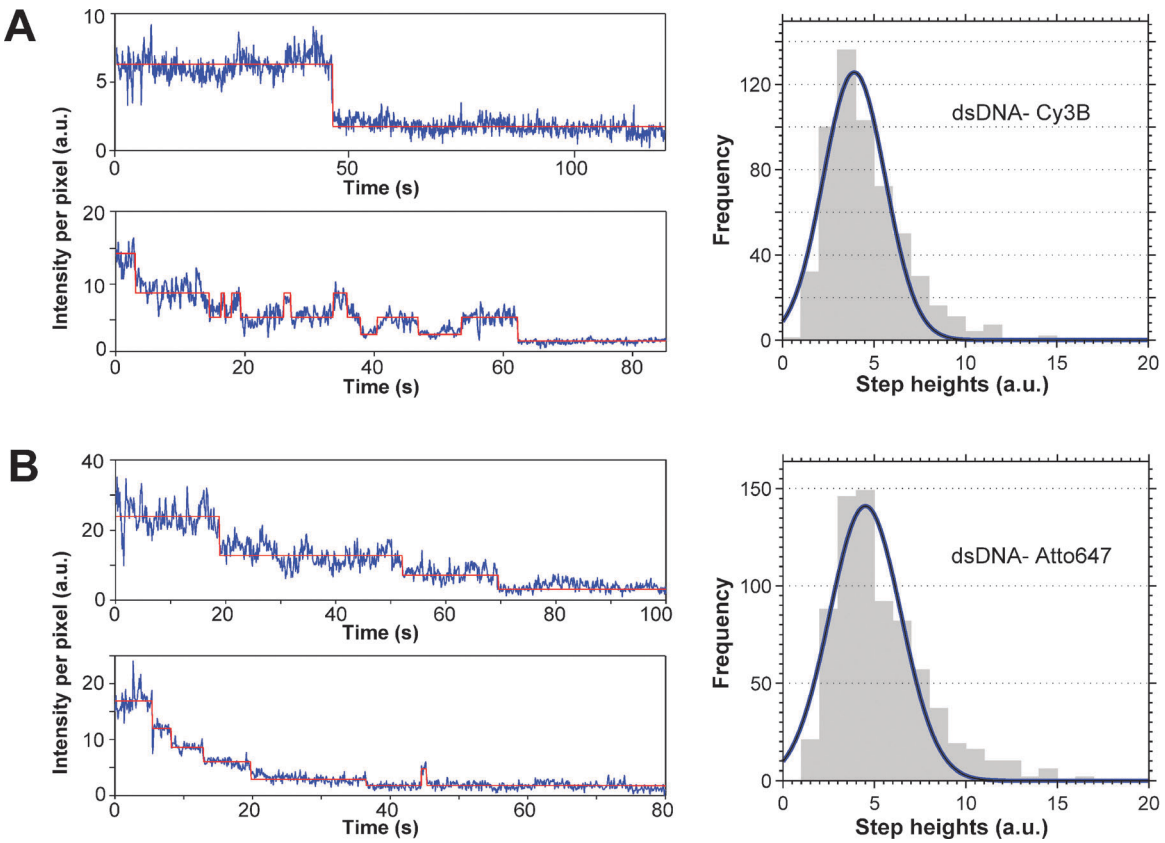

Fig. 3 Brightness study of organic fluorophores *in vivo*. Single-cell photobleaching step size analysis as a measure of fluorophore brightness in live *E. coli*. (A) Internalization of dsDNA-Cy3B and single-cell photobleaching step size analysis. Left: an example of single-cell photobleaching timetraces (blue: raw data, red: HMM fit). Right: a histogram of single-step height intensities from fitted steps (~100 cells). The single-Gaussian fit (blue) is centered at (3.9 ± 1.7) a.u., corresponding to a unitary fluorophore intensity of (3400 ± 1500) photons per second. (B) Internalization of dsDNA-Atto647 and single-cell photobleaching step size analysis. Left: an example of single-cell photobleaching timetraces (blue: raw data, red: HMM fit). Right: a histogram of single-step height intensities from fitted steps (~100 cells). The single-Gaussian fit (blue) is centered at (4.5 ± 2.0) a.u., corresponding to a unitary fluorophore intensity of (3900 ± 1700) photons per second.

for up to 100 cells (Fig. 3, left, blue curves: raw data, red curves: HMM fit). The center of a single Gaussian fit of the binned photobleaching step heights is the unitary fluorophore intensity, and corresponds to the *in vivo* brightness of a single fluorophore (Fig. 3, right). We obtained a brightness value of (3400 ± 1500) photons per second for Cy3B and (3900 ± 1700) photons per second for Atto647.

The brightness of mCherry could not be obtained under these illumination conditions, since at such low copy numbers, the single-cell photobleaching timetraces were too noisy and no single-step bleaching events were picked up by HMM analysis. For dsDNA-Cy3, we still detected single photobleaching steps using HMM analysis and obtained a brightness value of about 2800 photons per second (Fig. S5A, ESI†). Thus, we concluded that the brightness of mCherry is lower than 2800 photons per second.

The fluorophore performance after photostability and brightness analysis is summarized in Table 1 and the organic fluorophores are evaluated for their use in *in vivo* single-molecule fluorescence and FRET studies. At this point, long observation times and a high localization precision are the main requirements of the organic fluorophore for our *in vivo* FRET studies. Thus, very photostable and bright organic dyes aid towards obtaining long single-molecule FRET timetraces with very high localization precision, since lateral localization precision scales with $1/\sqrt{N}$ where N is the number of photons per frame.[17] Evaluating the dye performance using these

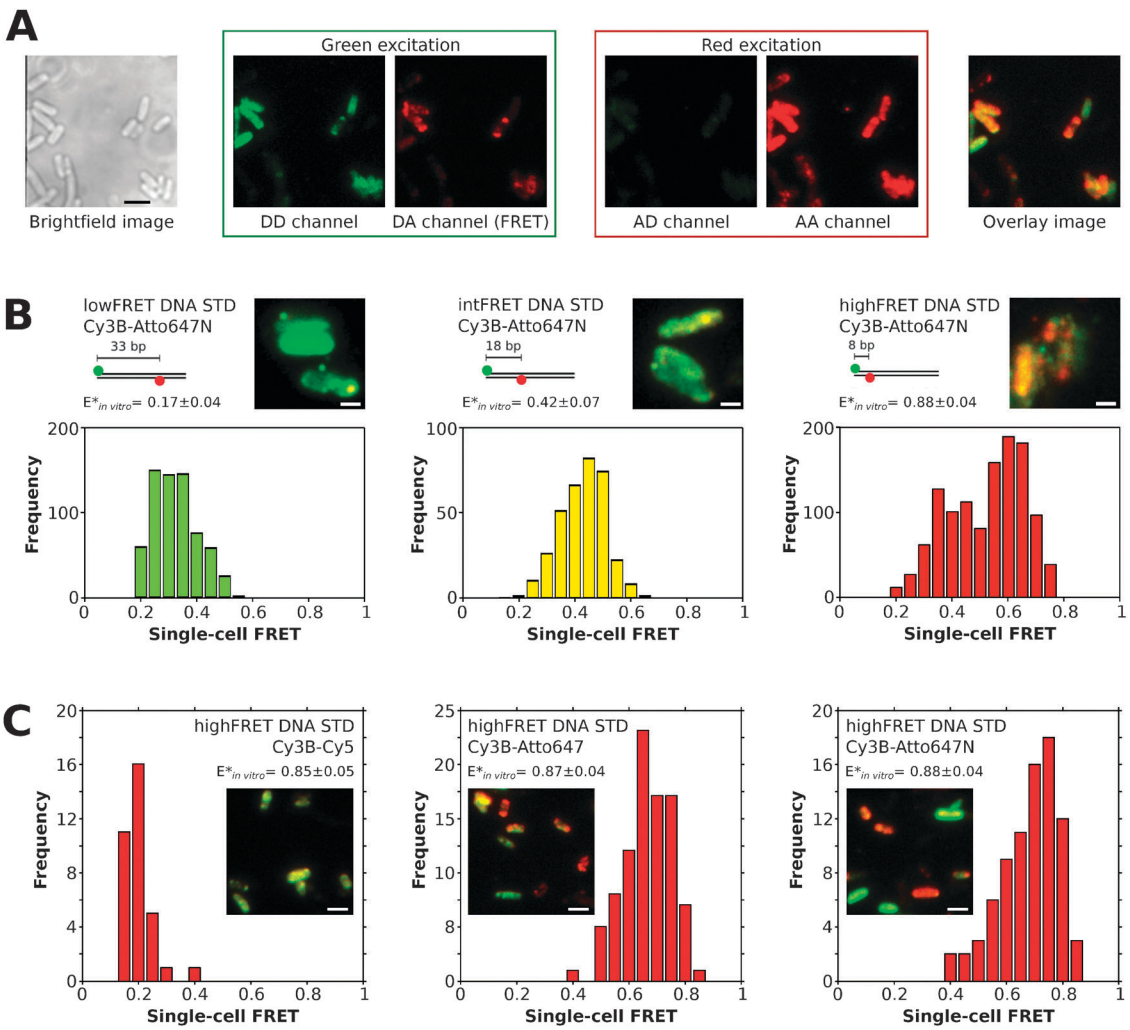

Fig. 4 *In vivo* single-cell FRET studies using an alternating laser excitation (ALEX) scheme. (A) Example FOV illustrates switching of green and red excitations and fluorescence data acquisition during one cycle. Left: a brightfield image of cells. Green box: donor (D) and acceptor (A) emission channels upon donor excitation; DD and DA/FRET channels, respectively. Red box: donor and acceptor emission channels upon acceptor excitation; AD and AA channels, respectively. Right: an overlay image of the DD channel (green) and the DA channel (red) encoding the FRET signature in a color-code: green-yellow-red visualizes low, intermediate and high FRET signals. Scale bar: 3 μm. (B) Automated single-cell FRET analysis of low, intermediate and high FRET DNA standards (left to right) in live *E. coli*. Top: overlay images of three example FOVs and *in vitro* FRET values. Bottom: histograms of single-cell FRET values obtained by automated cell segmentation and corrected for overall autofluorescence of non-treated cells (ESI†). Scale bar: 1 μm. (C) Manual single-cell FRET analysis of high FRET DNA standards labeled with Cy3B–Cy5, Cy3B–Atto647 and Cy3B–Atto647N (left to right). Insets: overlay images of example FOVs showing heterogeneity within single-cell FRET signals. Main: histograms of single-cell FRET values obtained by manual cell selection of cells showing high DA signals and locally corrected for autofluorescence (ESI†). Scale bar: 3 μm.

criteria, we selected Cy3B–Atto647 and Cy3B–Atto647N as FRET dye pairs and used these two FRET dye pairs in our single-cell FRET studies.

In vivo single-cell FRET studies

The idea of single-cell FRET studies is to evaluate different FRET states or FRET changes on the overall cell level. The evaluation of FRET at the cell level is much easier than working at the single-molecule level, and could also be used to get a quick overall picture of your system of interest in live bacteria. We used low, intermediate and high FRET DNA standards with *in vitro* single-molecule FRET values of ~17%, ~42% and ~88% (Fig. S1, ESI†) and used an alternating laser excitation scheme (ALEX; ref. 18). ALEX gives direct access to the stoichiometry of donor-only, acceptor-only and FRET populations and thus is of great use for initial single-cell FRET characterization.

To characterize FRET at the cell level, we electroporated *E. coli* with 1 μM dsDNA FRET standards Cy3B–Atto647N; Fig. 4A shows an example field-of-view using an ALEX scheme. Using automated cell segmentation and FRET analysis routines (ESI†), *in vivo* single-cell FRET distributions (Fig. 4B) were in good agreement with expected *in vitro* FRET values. The difference between low, intermediate and high single-cell FRET distributions is smaller than that for the *in vitro* values; we attribute the difference to an overall correction for cellular autofluorescence of non-treated cells used throughout the whole data set in the automated analysis. Especially, the single-cell FRET values for the high FRET DNA standard show a very wide distribution, which could also be explained due to faster acceptor photobleaching and DNA degradation.

To look into this in more detail, we electroporated different high FRET DNA standards such as dsDNA Cy3B–Cy5, Cy3B–Atto647 and Cy3B–Atto647N with *in vitro* single-molecule FRET values of ~85%, ~87% and ~88% (Fig. S1, ESI†) and carried out single-cell FRET studies using an ALEX scheme. We manually analyzed cells showing high signals in the DA/FRET channel and thus potentially high single-cell FRET values (Fig. 4C). Having fewer statistics, we were still able to retrieve high single-cell FRET populations for Cy3B–Atto647 and Cy3B–Atto647N DNA FRET standards (Fig. 4C, middle and right). A donor-only population was observed for Cy3B–Cy5 due to fast acceptor photobleaching, photoswitching and leakage of donor fluorophore signals into the FRET channel, which appeared as a FRET signal. This is in good agreement with photostability studies in Fig. S3, ESI† and Table 1, where we observed 5-fold to 10-fold faster photobleaching of Cy5 compared to Atto647 and Atto647N, respectively.

Nevertheless, we obtained benchmarks for *in vivo* single-cell FRET studies using Cy3B–Atto647 and Cy3B–Atto647N as FRET dye pairs and were able to differentiate low, intermediate and high single-cell FRET states *in vivo*. This single-cell FRET assay provides an attractive way to study intramolecular changes in biomolecules or intermolecular interactions of biomolecules (binding and unbinding, complex formation) on the cellular basis over hundreds of living cells at a time.

Conclusions

First, we studied the viability and loading of electroporated cells dependent on the applied electric field strength for six different electroporation voltages. We were able to maintain a viability of 70% at 1.4 kV and 1.6 kV, and obtained more than 60% loading at 1.8 kV. Cellular loading was studied 1.5 h after electroporation and cell recovery where the cellular fluorescence cuts in half with each division cycle (~30 min division time). Looking at loading of dsDNA standards directly after electroporation with only a 20 min recovery time, we previously achieved internalization efficiencies of >90% at 1.8 kV.[1]

Second, we studied the photostability and brightness of seven organic fluorophores using single-cell photobleaching studies. The organic fluorophores showed similar brightness and Cy3B, Atto647 and Atto647N performed best; showing photobleaching lifetimes of about 20 s, 45 s and 90 s. We would like to mention that Atto647N is hydrophobic and thus is known to stick to cell membranes, which has to be checked for any *in vivo* study.[19] The presented single-cell photobleaching analysis can be used as a general method to screen for labels (organic fluorophores or fluorescent proteins) for their use in single-cell and single-molecule fluorescence studies in live cells.

In our single-cell FRET studies we used Cy3B–Atto647 and Cy3B–Atto647N as FRET dye pairs. We were able to distinguish low, intermediate and high FRET states *in vivo* using dsDNA FRET standards. While characterizing single-cell FRET signals using DNA FRET standards, we faced two problems, (i) fast acceptor photobleaching and (ii) DNA degradation, which both led to the decrease of FRET signals at the cell level.

DNA degradation could be caused by the recognition of blunt DNA ends as DNA breaks or short dsDNA fragments as non-endogenous molecules by endonucleases. In further studies, this could be overcome by using protected DNA standards where the two DNA strands are chemically linked on both ends or by using small doubly-labeled proteins as FRET standards. Since the internalization of proteins *via* electroporation cannot be generally treated and often requires certain optimization steps,[20] electroporating doubly-labeled dsDNA is still the best option to characterize FRET signals in live bacteria.

Single-cell FRET studies provide an easy-to-use and quick assay to study intramolecular or intermolecular changes at an ensemble level within many cells and thus could be used to study for instance complex formation, protein–protein interactions, and gene expression. Such single-cell FRET studies allow a quick screening of FRET states of many cells over many generations.

The next step is to study FRET at the single-molecule level in living bacteria to investigate molecular heterogeneity and links for instance conformational changes, *i.e.* changes in FRET, with molecular diffusion and the spatial organization of the biomolecules of interest. Here again, the use of an alternating laser excitation scheme is beneficial, since it gives direct access

to donor and acceptor-only species and enables us to correct single-molecule FRET values for donor and acceptor leakage into the respective other fluorescence channels.[18]

Acknowledgements

We would like to thank Marko Sustarsic and Louise Aigrain for fruitful discussions. A.P. was supported by the Engineering and Physical Sciences Research Council (EPSRC) and the German National Academic Foundation (Studienstiftung). R.C. held an EPA Cephalosporin Junior Research Fellowship at Linacre College, Oxford and A.K. was supported by a UK BBSRC grant (BB/H01795X/1), and a European Research Council Starter grant (261227).

Notes and references

1 R. Crawford, J. P. Torella, L. Aigrain, A. Plochowietz, K. Gryte, S. Uphoff and A. N. Kapanidis, *Biophys. J.*, 2013, **105**, 2439–2450.
2 X. S. Xie, P. J. Choi, G. W. Li, N. K. Lee and G. Lia, *Annu. Rev. Biophys.*, 2008, **37**, 417–444.
3 E. A. Lipman, B. Schuler, O. Bakajin and W. A. Eaton, *Science*, 2003, **301**, 1233–1235.
4 J. Hohlbein, L. Aigrain, T. D. Craggs, O. Bermek, O. Potapova, P. Shoolizadeh, N. D. Grindley, C. M. Joyce and A. N. Kapanidis, *Nat. Commun.*, 2013, **4**, 2131.
5 Y. Santoso, C. M. Joyce, O. Potapova, L. Le Reste, J. Hohlbein, J. P. Torella, N. D. Grindley and A. N. Kapanidis, *Proc. Natl. Acad. Sci. U. S. A.*, 2010, **107**, 715–720.
6 N. C. Shaner, P. A. Steinbach and R. Y. Tsien, *Nat. Methods*, 2005, **2**, 905–909.
7 R. Y. Tsien, *Annu. Rev. Biochem.*, 1998, **67**, 509–544.
8 G. T. Dempsey, J. C. Vaughan, K. H. Chen, M. Bates and X. Zhuang, *Nat. Methods*, 2011, **8**, 1027–1036.
9 P. L. McNeil, R. F. Murphy, F. Lanni and D. L. Taylor, *J. Cell Biol.*, 1984, **98**, 1556–1564.
10 M. S. Clarke and P. L. McNeil, *J. Cell Sci.*, 1992, **102**(Pt 3), 533–541.
11 D. L. Taylor and Y. L. Wang, *Proc. Natl. Acad. Sci. U. S. A.*, 1978, **75**, 857–861.
12 J. J. Sakon and K. R. Weninger, *Nat. Methods*, 2010, **7**, 203–205.
13 T. Fessl, F. Adamec, T. Polivka, S. Foldynova-Trantirkova, F. Vacha and L. Trantirek, *Nucleic Acids Res.*, 2012, **40**, e121.
14 E. Neumann, M. Schaefer-Ridder, Y. Wang and P. H. Hofschneider, *EMBO J.*, 1982, **1**, 841–845.
15 Y. Song, T. Hahn, I. P. Thompson, T. J. Mason, G. M. Preston, G. Li, L. Paniwnyk and W. E. Huang, *Nucleic Acids Res.*, 2007, **35**, e129.
16 Y. Sako, S. Minoghchi and T. Yanagida, *Nat. Cell Biol.*, 2000, **2**, 168–172.
17 R. E. Thompson, D. R. Larson and W. W. Webb, *Biophys. J.*, 2002, **82**, 2775–2783.
18 N. K. Lee, A. N. Kapanidis, Y. Wang, X. Michalet, J. Mukhopadhyay, R. H. Ebright and S. Weiss, *Biophys. J.*, 2005, **88**, 2939–2953.
19 K. Kolmakov, V. N. Belov, J. Bierwagen, C. Ringemann, V. Muller, C. Eggeling and S. W. Hell, *Chem. – Eur. J.*, 2010, **16**, 158–166.
20 M. Sustarsic, A. Plochowietz, L. Aigrain, Y. Yuzenkova, N. Zenkin and A. Kapanidis, *Histochem. Cell Biol.*, 2014, DOI: 10.1007/s00418-014-1213-2.